

ProDMPs: A Unified Perspective on Dynamic and Probabilistic Movement Primitives

Ge Li¹, Zeqi Jin¹, Michael Volpp¹, Fabian Otto^{2,3}, Rudolf Lioutikov¹, and Gerhard Neumann¹

Abstract—Movement Primitives (MPs) are a well-known concept to represent and generate modular trajectories. MPs can be broadly categorized into two types: (a) dynamics-based approaches that generate smooth trajectories from any initial state, e.g., Dynamic Movement Primitives (DMPs), and (b) probabilistic approaches that capture higher-order statistics of the motion, e.g., Probabilistic Movement Primitives (ProMPs). To date, however, there is no method that unifies both, i.e. that can generate smooth trajectories from an arbitrary initial state while capturing higher-order statistics. In this paper, we introduce a unified perspective of both approaches by solving the ODE underlying the DMPs. We convert expensive online numerical integration of DMPs into basis functions that can be computed offline. These basis functions can be used to represent trajectories or trajectory distributions similar to ProMPs while maintaining all the properties of dynamical systems. Since we inherit the properties of both methodologies, we call our proposed model Probabilistic Dynamic Movement Primitives (ProDMPs). Additionally, we embed ProDMPs in deep neural network architecture and propose a new cost function for efficient end-to-end learning of higher-order trajectory statistics. To this end, we leverage Bayesian Aggregation for non-linear iterative conditioning on sensory inputs. Our proposed model achieves smooth trajectory generation, goal-attractor convergence, correlation analysis, non-linear conditioning, and online re-planning in one framework.

I. INTRODUCTION

Movement Primitives (MPs) are a prominent tool for motion representation and synthesis in robotics. They serve as basic movement elements, modulate the motion behavior, and form more complex movements through combination or concatenation. This work focuses on trajectory-based movement representations [1, 2]. Given a parameter vector, such representations generate desired trajectories for the robot to follow. These methods have gained much popularity in imitation and reinforcement learning (IL, RL) [3–7] due to their concise parametrization and flexibility to modulate movement. Current methods can be roughly classified into approaches based on dynamical systems [1, 8–11] and probabilistic approaches [2, 12, 13], with both types offering their own advantages. The dynamical systems-based approaches, such as Dynamic Movement Primitives (DMPs), guarantee that the generated trajectories start precisely at the current position and velocity of the robot, which allows for smooth trajectory replanning i.e., changing the parameters of the MPs during motion execution [11, 14]. However, since DMPs represent the trajectory via the forcing term instead of a direct representation of the trajectory position, numerical

integration from acceleration to position has to be applied to formulate the trajectory, which constitutes an additional workload and makes the estimation of the trajectory statistics difficult [15]. Probabilistic methods, such as Probabilistic Movement Primitive (ProMP), are able to acquire such statistics, thus making them the key enablers for acquiring variable-stiffness controllers and the trajectory’s temporal and DoFs correlation. These methods further perform as generative models, facilitating the sampling of new trajectories. However, the lack of internal dynamics of these approaches suffers from discontinuities in position and velocity between old and new trajectories in the case of replanning.

In this work, we propose Probabilistic Dynamic Movement Primitives (ProDMPs) which unify both methodologies. We show that the trajectory of a DMP, obtained by integrating its second-order dynamical system, can be expressed by a linear basis function model that depends on the parameters of the DMP, i.e., the weights of the forcing function and the goal attractor. The linear basis functions can be obtained by integrating the original basis functions used in the DMP - an operation that only needs to be performed once offline in the ProDMPs. Recently, MP research has been extended to deep neural network (NN) architectures [10, 11, 13] that enable conditioning the trajectory generation on high-dimensional context variables, such as images. Following these ideas, we integrate our representation into a deep neural architecture that allows non-linear conditioning on a varying number of conditioning events. These events are aggregated using Bayesian Aggregation (BA) into a latent probabilistic representation [16] which is mapped to a Gaussian distribution in the parameter space of the ProDMPs. We summarize the contributions of this paper as: (a) We unify ProMPs and DMPs into one consistent framework that inherits the benefits of both formulations. (b) We enable to compute distributions and to capture correlations of DMPs trajectories, while (c) the robot’s current state can be inscribed into the trajectory distribution through boundary conditions, allowing for smooth replanning. (d) Moreover, the offline integration of the basis functions significantly facilitates the integration into neural network architectures, reducing the computation time by a factor of 10. (e) Hence, we embed ProDMPs in a deep encoder-decoder architecture that allows non-linear conditioning on a set of high-dimensional observations with varying information levels. We evaluate our method on three digit-writing tasks using images as inputs, a simulated robot pushing task with a complex physical interaction, and a real robot picking task with shifting object positions. We compare our model with state-of-the-art NN-based DMPs [9–11] and

¹Karlsruhe Institute of Technology, Germany. ge.li@kit.edu

²Bosch Center for Artificial Intelligence, Germany.

³University of Tübingen, Germany.

the NN-based probabilistic method [13].

II. RELATED WORK

Paraschos et al. [2] established ProMPs to model MPs as a trajectory distribution that captures temporal correlation and correlations between the DoFs. ProMPs maintain a Gaussian distribution over the parameters and can map it to the corresponding trajectory distribution using a linear basis function model. In contrast, such a distribution mapping is not allowed for the DMP-based approaches, as the trajectory is integrated numerically from the forcing function. Previous methods, like GMM/GMR-DMPs [17, 18] used Gaussian Mixture Models to cover the trajectories’ domain. Yet, this does not capture temporal correlation nor does it provide a generative approach to trajectories. Other methods which have learned distributions over DMP weights [19, 20], do not connect the weights distribution to the trajectory distribution, as trajectories can only be obtained by integration. Hence, it is also hard to learn the weights distribution reversely from trajectories in an end-to-end manner.

To learn DMP parameters from high-dimensional sensory inputs, Gams et al. [9] and Ridge et al. [10] designed an encoder-decoder architecture to learn the weights of a single DMP from digit images, and derive the gradient of the trajectory with respect to the learnable parameters. Bahl et al. [11] propose Neural Dynamic Policies (NDP) that allow replanning the DMP parameters throughout the execution of the trajectory which has also been extended to the RL setting. The learning objective of these two methods for IL is to optimize the mean squared error (MSE) between the predicted and the ground-truth trajectories using backpropagation. However, to formulate a trajectory, DMPs must apply numerical integration during the NN training procedure, which significantly increases the computational workload in both forward and backward propagation, rendering these approaches cumbersome to use. Additionally, the integration-based trajectory representation limits the use of probabilistic methods and hence these NN-DMPs approaches cannot be trained using a probabilistic log-likelihood (LL) loss.

Probabilistic MPs approaches have also been extended with deep NN architectures. Seker et al. [13] directly use a Conditional Neural Processes model [21] as a trajectory generator, i.e. Conditional Neural Movement Primitives (CNMPs), to predict the trajectory distribution with an encoder-decoder NNs model. While such an architecture enables non-linear conditioning on high-dimensional inputs, it can only predict an isotropic trajectory variance at each time step. The temporal and DoFs correlations are missing, which makes sampling consistently in time and DoFs infeasible. Besides, both ProMPs and CNMPs neglect dynamics, i.e., when changing trajectory parameters during trajectory execution, the newly generated trajectory will contain discontinuities at the replanning time point. To execute such trajectories, a heuristic controller is used to freeze the time and catch up with the jump [13]. However, such a waiting mechanism does not scale to time-sensitive motions and tasks.

III. A UNIFIED PERSPECTIVE ON DYNAMIC AND PROBABILISTIC MOVEMENT PRIMITIVES

We first briefly cover the fundamental aspects of DMPs. Then, we derive the analytical solution of the DMPs’ ODE to develop our new ProDMPs representation. For convenience, we introduce our approach through a 1-DoF dynamical system and later extend it to a high-DoFs system.

A. Solving DMPs’ Ordinary Differential Equation

For a single movement execution as a trajectory $\lambda = [y_t]_{t=0:T}$, Schaal [1] and Ijspeert et al. [8] model it as a second-order linear dynamical system with a non-linear forcing function f ,

$$\tau^2 \ddot{y} = \alpha(\beta(g-y) - \tau \dot{y}) + f(x), \quad f(x) = x \frac{\sum \varphi_i(x) w_i}{\sum \varphi_i(x)} = x \varphi_x^T \mathbf{w}, \quad (1)$$

where $y = y(t)$, $\dot{y} = dy/dt$, $\ddot{y} = d^2y/dt^2$ represent the position, velocity, and acceleration of the system at time step t , respectively. Here, we use the original formulation of DMPs in [1] without any extensions. α and β are spring-damper constants, g is a goal attractor, and τ is a time constant which can be used to adapt the execution speed of the resulting trajectory. To this end, DMPs define the forcing function over an exponentially decaying phase variable $x(t) = \exp(-\alpha_x/\tau t)$, where $\varphi_i(x)$ represents the (unnormalized) basis functions and $w_i \in \mathbf{w}$, $i = 1 \dots N$ are the corresponding weights. The trajectory of the motion λ is obtained by integrating the dynamical system, or more specifically, numerical integration from starting time to the target time point. The dynamical system defined in Eq. (1) is a second-order linear non-homogeneous ordinary differential equation (ODE) with constant coefficients, whose closed-form solution can be derived analytically. We rewrite the ODE and its homogeneous counterpart in standard form as

$$\text{DMPs' ODE: } \ddot{y} + \frac{\alpha}{\tau} \dot{y} + \frac{\alpha\beta}{\tau^2} y = \frac{f(x)}{\tau^2} + \frac{\alpha\beta}{\tau^2} g \equiv F(x, g), \quad (2)$$

$$\text{Homo. ODE: } \ddot{y} + \frac{\alpha}{\tau} \dot{y} + \frac{\alpha\beta}{\tau^2} y = 0, \quad (3)$$

where F denotes some function of x and g . Using the method of variation of constants [22], the closed-form solution of the second-order ODE in Eq. (2), i.e., the trajectory position, is

$$y = c_1 y_1 + c_2 y_2 - y_1 \int \frac{y_2 F}{Y} dt + y_2 \int \frac{y_1 F}{Y} dt, \quad (4)$$

where y_1, y_2 are two linearly independent complementary functions of the homogeneous ODE given in Eq. (3). c_1, c_2 are two constants which are determined by the boundary conditions (BCs) of the ODE, and $Y = y_1 \dot{y}_2 - \dot{y}_1 y_2$. Both integrals in Eq. (4) are indefinite. With appropriate values $\beta = \alpha/4$ [1, 8], the system is critically damped, and the corresponding characteristic equation of the homogeneous ODE, i.e. $\Delta = (\alpha^2 - 4\alpha\beta)/\tau^2$ will be 0. Consequently, y_1, y_2 will take the form

$$y_1 = y_1(t) = \exp\left(-\frac{\alpha}{2\tau} t\right), \quad y_2 = y_2(t) = t \exp\left(-\frac{\alpha}{2\tau} t\right). \quad (5)$$

Using this result, the term Y can also be simplified to $Y = \exp(-\alpha t/\tau) \neq 0$. To get y , we need to solve the two

indefinite integrals in Eq. (4) as

$$\begin{aligned} I_1(t) &= \int \frac{y_2 F}{Y} dt = \int t \exp\left(\frac{\alpha}{2\tau} t\right) F(x, g) dt, \\ I_2(t) &= \int \frac{y_1 F}{Y} dt = \int \exp\left(\frac{\alpha}{2\tau} t\right) F(x, g) dt. \end{aligned} \quad (6)$$

Applying the Fundamental Theorem of Calculus, i.e., $\int h(t) dt = \int_0^t h(t') dt' + c$, $c \in \mathbb{R}$, together with the definition of the forcing function f in Eq. (1) and $F(x, g)$ in Eq. (2), $I_1(t)$ can be expressed as

$$I_1(t) = \frac{1}{\tau^2} \left[\int_0^t t' \exp\left(\frac{\alpha}{2\tau} t'\right) x(t') \varphi_x^T \mathbf{w} dt' + \int_0^t t' \exp\left(\frac{\alpha}{2\tau} t'\right) \frac{\alpha^2}{4} g dt' \right] + c_3 \quad (7)$$

$$\begin{aligned} &= \frac{1}{\tau^2} \left[\int_0^t t' \exp\left(\frac{\alpha}{2\tau} t'\right) x(t') \varphi_x^T dt' \right] \mathbf{w} \\ &\quad + \left[\left(\frac{\alpha}{2\tau} t - 1\right) \exp\left(\frac{\alpha}{2\tau} t\right) + 1 \right] g + c_3, \end{aligned} \quad (8)$$

where c_3 is a constant fixed by the BCs. From Eq. (7) to Eq. (8), we move the time-independent parameters \mathbf{w} and g out of their corresponding integrals. Notice that the remaining part of the second integral has an analytical solution. The remaining part of the first integral, however, has no closed-form solution because the basis functions φ_x may be arbitrarily complex. Denoting these integrals as

$$\begin{aligned} \mathbf{p}_1(t) &\equiv \frac{1}{\tau^2} \int_0^t t' \exp\left(\frac{\alpha}{2\tau} t'\right) x(t') \varphi_x^T dt', \\ q_1(t) &\equiv \left(\frac{\alpha}{2\tau} t - 1\right) \exp\left(\frac{\alpha}{2\tau} t\right) + 1, \end{aligned} \quad (9)$$

where \mathbf{p}_1 is a N-dim vector and q_1 a scalar, we can express $I_1(t) = \mathbf{p}_1(t)^T \mathbf{w} + q_1(t)g + c_3$. Following the same steps, we can obtain a similar solution for I_2 , i.e., $I_2(t) = \mathbf{p}_2(t)^T \mathbf{w} + q_2(t)g + c_4$, where we present $\mathbf{p}_2(t)$ and $q_2(t)$ in Eq. (10).

$$\begin{aligned} \mathbf{p}_2(t) &= \frac{1}{\tau^2} \int_0^t \exp\left(\frac{\alpha}{2\tau} t'\right) x(t') \varphi_x^T dt', \\ q_2(t) &= \frac{\alpha}{2\tau} \left[\exp\left(\frac{\alpha}{2\tau} t\right) - 1 \right] \end{aligned} \quad (10)$$

B. DMPs' Linear Basis Functions Representation.

Substituting the two integrals I_1 and I_2 in Eq. (4) by their derived form, the constants c_3 and c_4 can then be merged into c_1 and c_2 , respectively. We can now express the position of DMPs in Eq. (4) as a summation of complementary functions y_1 and y_2 , plus a linear basis function representation of the weights \mathbf{w} and the goal attractor g

$$\begin{aligned} y &= c_1 y_1 + c_2 y_2 + \begin{bmatrix} y_2 \mathbf{p}_2 - y_1 \mathbf{p}_1 & y_2 q_2 - y_1 q_1 \end{bmatrix} \begin{bmatrix} \mathbf{w} \\ g \end{bmatrix} \\ &\equiv c_1 y_1 + c_2 y_2 + \Phi^T \mathbf{w}_g, \end{aligned} \quad (11)$$

where \mathbf{w}_g is a N+1-dim vector containing the weights \mathbf{w} and the goal g . The resulting basis functions for \mathbf{w} and g are represented by $\Phi(t)$, which can be solved numerically, cf. Fig. 1. The constants c_1 and c_2 are determined by solving a boundary condition problem where we use the current position and velocity of the robot to inscribe where the trajectory should start.

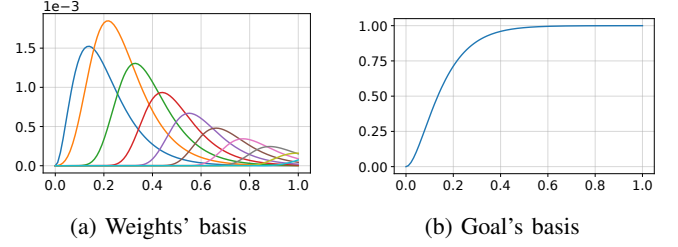


Fig. 1: The basis functions Φ of the ProDMPs can be computed offline and later used in online trajectory generation.

Online:



(a) NN + DMPs couple the numerical integration and the learning.

Offline, computed once: $\rightarrow \Phi$

Online:



(b) NN + ProDMPs decouple the numerical integration from the learning pipeline and can also model trajectory distributions.

Fig. 2: Comparison of trajectory generation pipelines between (a) NN-based DMPs [9–11] and (b) ProDMPs. The node **DNN** represents arbitrary deep neural network architecture. The blue arrows denote the learning pipeline while the red arrows the numerical integration. Our method transforms the expensive numerical integration as basis functions computed offline which speeds up the trajectory computation and allows trajectory distribution prediction.

TABLE I: Computation time of both pipelines. Here a 2-DoFs, 6-seconds long, 1000 Hz trajectory is generated from a 22-dim \mathbf{w}_g parameter vector. We tested both forward pass (**FP**) and backward pass (**BP**). A 3-layer fully connected (FC) network with [10, 128, 22] neurons on input, hidden and output layers respectively are used to simulate the learning procedure. The keyword **+BC** are the settings where the boundary conditions are renewed so that the coefficients c_1 and c_2 need to be recomputed. Otherwise, they remain unchanged. The result shows that our model is 200-4600 times faster than the NN-DMPs in different settings. We use a Nvidia® RTX-3080Ti GPU for our test. In a full learning experiment with NN architectures, this speed difference translates into a speed-up of around 10 times (see experiments).

Pipelines	FP	FP + BC	BP	BP + BC
NN-DMPs	0.6057 s	0.6145 s	1.5261 s	1.5737 s
ProDMPs	0.00013 s	0.0027 s	0.00105 s	0.0039 s
Speed-up	× 4659	× 227	× 1453	× 403

In contrast to previous NN-DMPs methods [9–11], our model separates the learnable parameters from the numerical integrals which are transformed as basis functions. These basis functions are shared by all trajectories to be generated during learning procedure. Hence, we can pre-compute these basis functions once offline at first and use them as constants in online trajectory generation. Consequently, we exclude numerical integrals from forward and backward propagation

of NN pipelines, and significantly increase the trajectory generation speed. We present a pipeline comparison and corresponding speed test between previous methods and our ProDMPs in Fig. 2 and TABLE I.

C. Solving the Boundary Condition Problem

To compute the coefficients c_1 and c_2 , we need to first obtain the velocity representation by computing the derivative of Eq. (4) w.r.t. time. The resulting equation reads

$$\dot{y} = c_1 \dot{y}_1 + c_2 \dot{y}_2 - \dot{y}_1 \int \frac{y_2 F}{Y} dt + \dot{y}_2 \int \frac{y_1 F}{Y} dt. \quad (12)$$

Note that Eq. (4) and Eq. (12) share a similar structure using the same constants c_1 and c_2 , as well as the two indefinite integrals in Eq. (6). The only difference is that the two complementary functions y_1 and y_2 are replaced by their derivatives \dot{y}_1 and \dot{y}_2 . By reusing the derivation of Eq. (6, 8, 9, 10), the trajectory velocity is ultimately represented by

$$\begin{aligned} \dot{y} &= c_1 \dot{y}_1 + c_2 \dot{y}_2 + \begin{bmatrix} \dot{y}_2 \mathbf{p}_2 - \dot{y}_1 \mathbf{p}_1 \dot{y}_2 q_2 - \dot{y}_1 q_1 \\ \mathbf{w} \\ g \end{bmatrix} \\ &\equiv c_1 \dot{y}_1 + c_2 \dot{y}_2 + \dot{\Phi}^\top \mathbf{w}_g, \end{aligned} \quad (13)$$

where $\dot{\Phi}(t)$ represents the basis functions of the velocity. The position and velocity in Eq. (11, 13) share the same linear model structure, coefficients c_1, c_2 , and the parameters \mathbf{w}_g .

We need two boundary conditions to solve c_1 and c_2 . Theoretically, there are three options, (a) two boundary position values at two time steps, i.e. $y(t_{b_1}), y(t_{b_2}), t_{b_1} \neq t_{b_2}$, (b) two boundary velocity values at two time steps, i.e. $\dot{y}(t_{b_1}), \dot{y}(t_{b_2}), t_{b_1} \neq t_{b_2}$, and (c) one boundary position value plus one boundary velocity value $y(t_{b_1}), \dot{y}(t_{b_2})$, where t_{b_1} and t_{b_2} are typically identical. The third option allows us to naturally integrate the current position and velocity of a robot as boundary conditions of a trajectory to be generated. We denote the boundary conditions as a position and velocity pair (y_b, \dot{y}_b) at time step t_b . The values of the complementary functions in Eq. (5) and their corresponding derivatives at t_b are denoted by $y_{1_b}, y_{2_b}, \dot{y}_{1_b}, \dot{y}_{2_b}$. The value of the position basis and velocity basis at t_b are denoted as $\Phi_b, \dot{\Phi}_b$. By substituting these terms into Eq. (11, 13), we can solve

$$\begin{bmatrix} c_1 \\ c_2 \end{bmatrix} = \begin{bmatrix} \frac{\dot{y}_{2_b} y_b - y_{2_b} \dot{y}_b}{y_{1_b} \dot{y}_{2_b} - y_{2_b} \dot{y}_{1_b}} + \frac{y_{2_b} \Phi_b^\top - \dot{y}_{2_b} \dot{\Phi}_b^\top}{y_{1_b} \dot{y}_{2_b} - y_{2_b} \dot{y}_{1_b}} \mathbf{w}_g \\ \frac{y_{1_b} \dot{y}_b - \dot{y}_{1_b} y_b}{y_{1_b} \dot{y}_{2_b} - y_{2_b} \dot{y}_{1_b}} + \frac{\dot{y}_{1_b} \Phi_b^\top - y_{1_b} \dot{\Phi}_b^\top}{y_{1_b} \dot{y}_{2_b} - y_{2_b} \dot{y}_{1_b}} \mathbf{w}_g \end{bmatrix}. \quad (14)$$

Substituting Eq. (14) into Eq. (11), we can express the trajectory position as

$$y = \xi_1 y_b + \xi_2 \dot{y}_b + [\xi_3 \Phi_b + \xi_4 \dot{\Phi}_b + \Phi]^\top \mathbf{w}_g, \quad (15)$$

where

$$\begin{aligned} \xi_1 = \xi_1(t) &= \frac{\dot{y}_{2_b} y_1 - \dot{y}_{1_b} y_2}{y_{1_b} \dot{y}_{2_b} - y_{2_b} \dot{y}_{1_b}}, & \xi_2 = \xi_2(t) &= \frac{y_{1_b} y_2 - y_{2_b} y_1}{y_{1_b} \dot{y}_{2_b} - y_{2_b} \dot{y}_{1_b}}, \\ \xi_3 = \xi_3(t) &= \frac{\dot{y}_{1_b} y_2 - \dot{y}_{2_b} y_1}{y_{1_b} \dot{y}_{2_b} - y_{2_b} \dot{y}_{1_b}}, & \xi_4 = \xi_4(t) &= \frac{y_{2_b} y_1 - y_{1_b} y_2}{y_{1_b} \dot{y}_{2_b} - y_{2_b} \dot{y}_{1_b}}. \end{aligned}$$

Eq. (15) shows that the trajectory position y is fully determined by the boundary position y_b , and velocity \dot{y}_b at the time step t_b , as well as the learnable weights \mathbf{w}_g .

D. Probability Distribution of Multi DoFs DMPs

The linear basis function representation of ProDMPs takes the same form of ProMPs. Hence, our model can also be extended to multi-DoFs systems $\mathbf{y} = [y^1, \dots, y^D]^\top$, where D denotes the system's DoFs. Similar to [2], we extend the basis functions $\Phi, \dot{\Phi}$, as well as their boundary values $\Phi_b, \dot{\Phi}_b$ to block-diagonal matrices $\Psi, \dot{\Psi}, \Psi_b, \dot{\Psi}_b$ and concatenate each DoF's boundary conditions into a vector, e.g., $y_b^1, \dots, y_b^D \rightarrow \mathbf{y}_b = [y_b^1, \dots, y_b^D]^\top$. Additionally, we note that the coefficient constants c_1 and c_2 of each DoF can be solved independently. As a consequence, we have the multi-DoFs trajectory as

$$\mathbf{y} = \xi_1 \mathbf{y}_b + \xi_2 \dot{\mathbf{y}}_b + [\xi_3 \Psi_b + \xi_4 \dot{\Psi}_b + \Psi]^\top \mathbf{w}_g, \quad (16)$$

Extending Eq. (16) from a single time step to the entire trajectory $\Lambda = [\mathbf{y}_t]_{t=0:T}$, we can now express the trajectory distribution similarly to ProMPs. We consider a system where the current robot state $\mathbf{y}_b, \dot{\mathbf{y}}_b$ can be acquired precisely, which is universal in most robotic systems. In this case, the trajectory's variability is only caused by the variability of the weights \mathbf{w}_g plus the observation white noise ϵ_y . Similar to ProMPs, assuming the weights \mathbf{w}_g follows a multivariate normal distribution $\mathbf{w}_g \sim \mathcal{N}(\mathbf{w}_g | \boldsymbol{\mu}_{\mathbf{w}_g}, \boldsymbol{\Sigma}_{\mathbf{w}_g})$, we can compute the trajectory distribution with full covariance over all time steps $0 : T$ and all DoFs $1 : D$ as

$$\begin{aligned} p(\Lambda; \boldsymbol{\mu}_{\mathbf{w}_g}, \boldsymbol{\Sigma}_{\mathbf{w}_g}, \mathbf{y}_b, \dot{\mathbf{y}}_b) &= \mathcal{N}(\Lambda | \boldsymbol{\mu}_\Lambda, \boldsymbol{\Sigma}_\Lambda), \\ \boldsymbol{\mu}_\Lambda &= \xi_1 \mathbf{y}_b + \xi_2 \dot{\mathbf{y}}_b + \mathbf{H}_{0:T}^\top \boldsymbol{\mu}_{\mathbf{w}_g}, \\ \boldsymbol{\Sigma}_\Lambda &= \mathbf{H}_{0:T}^\top \boldsymbol{\Sigma}_{\mathbf{w}_g} \mathbf{H}_{0:T} + \sigma_n^2 \mathbf{I}, \\ &\text{with } \mathbf{H}_{0:T} = \xi_3 \Psi_b + \xi_4 \dot{\Psi}_b + \Psi_{0:T} \end{aligned} \quad (17)$$

where $\xi_k = [\xi_k(t)]_{t=0:T}$. In a summary, ProDMPs unify DMPs and ProMPs in a consistent framework, inheriting the properties and advantages of both methodologies. In Fig. 3, we illustrate a few examples to highlight the properties. We show that ProDMPs using linear basis functions can generate an identical trajectory as DMPs, and enforce the predicted trajectory distribution adheres the given boundary conditions. The newly generated trajectories are guaranteed to have a smooth transition to the previous trajectory at the replanning time step. Furthermore, ProDMPs inherit all the probabilistic operations of ProMPs, such as combination and blending. For the exact formulations of these operations, we refer to the original ProMPs paper [2], as they remain unaltered.

IV. EMBED PRODMPs IN A DEEP ARCHITECTURE USING BAYESIAN SET ENCODERS

We extend ProDMPs with a deep NN architecture that allows for conditioning the trajectory distribution on a set of high-dimensional (time-stamped) sensory observations, such as images. Similar to recent MP architectures [13, 23], we treat such observations as set-inputs [24, 25], i.e., our architecture is invariant to the order of these observations.

Architecture. The architecture contains four major parts: encoder, aggregator, decoder, and the ProDMPs layer, cf. Fig. 4. The *Encoders* E_μ and E_{σ^2} of each sensor input type, e.g. images, compute for each observation $\mathbf{o}_m \in \mathcal{O}$ a corresponding latent observation \mathbf{r}_m and an uncertainty $\sigma_{r_m}^2$,

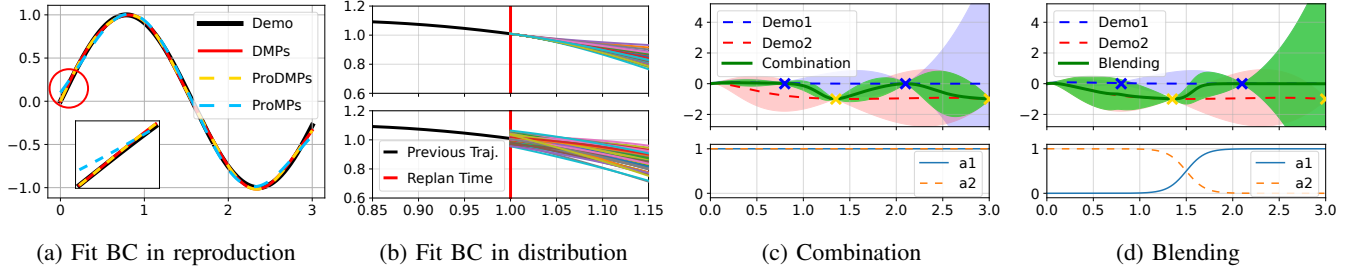


Fig. 3: Illustration of ProDMPs’ properties inherited from DMPs and ProMPs. (a) Given a demonstrated trajectory, ProDMPs can reproduce it and mathematically guarantee a fit of the boundary condition (BC), which cannot be guaranteed by ProMPs. Besides, ProDMPs reproduce the identical trajectory of DMPs’, given the same parameters w_g . As our method uses the linear basis functions rather than online numerical integration, it is thus much faster. (b) ProDMPs (upper) can model trajectory distributions and guarantee that all newly sampled trajectories follow the given boundary conditions, i.e. smooth online replanning. In the contrast, ProMPs’ samples (lower) cannot fit the boundary condition well, which often results in a jump in the case of replanning. (c) + (d) ProDMPs support probabilistic operations of ProMPs, e.g. combination and blending [2] of two demonstrated trajectory distributions (blue and red) into one resulting distribution (green).

measuring how informative this observation is. Different types of sensor inputs, e.g., images and robot states, are mapped via different types of encoders, e.g., CNN encoders and MLP encoders, into the same latent space. The *Bayesian Aggregation* [16] A is a parameter-free operator used to aggregate a set of latent observations $\{r_m\}$ and the corresponding uncertainties $\{\sigma_{r_m}^2\}$ into a latent state posterior $p(z|\mathcal{O})$ which is given by a factorized multivariate Gaussian distribution $\mathcal{N}(z|\mu_z, \sigma_z^2)$. The resulting aggregation is

$$\begin{aligned} \sigma_{z|\sigma_{1:M}}^2 &= \left[(\sigma_{z,0}^2)^\ominus + \sum_{m=1}^M (\sigma_{r_m}^2)^\ominus \right]^\ominus, \\ \mu_{z|\sigma_{1:M}} &= \mu_{z,0} + \sigma_z^2 \odot \sum_{m=1}^M (r_m - \mu_{z,0}) \oslash \sigma_{r_m}^2, \end{aligned} \quad (18)$$

where \ominus , \odot , and \oslash denote element-wise inversion, product, and division, respectively. The parameters of the latent variable’s prior distribution are $\mu_{z,0}$ and $\sigma_{z,0}^2$. Intuitively, BA takes the uncertainty of the different conditioning events into account which typically leads to better results than the mean aggregation [16]. Hence, we adopt this approach for our architecture. The *Decoders* D_μ, D_L predict the mean μ_{w_g} and the Cholesky decomposition L_{w_g} of the covariance Σ_{w_g} of the weights distribution. Similar to Volpp et al. [16], we do not sample from the latent posterior $p(z|\mathcal{O})$ but use its mean μ_z and variance σ_z^2 to predict μ_{w_g} and L_{w_g} , respectively. Given the query time steps $\{t\}$ and the current robot position y_b and velocity \dot{y}_b as boundary conditions, the *ProDMPs* layer computes the parameters μ_Λ and Σ_Λ of the trajectory distribution as a multivariate Gaussian distribution.

Loss Function. In this paper, we focus on Imitation Learning tasks and minimize the negative log-likelihood of the conditional trajectory distribution, i.e., $-\log \mathcal{N}(\Lambda|\mu_\Lambda, \Sigma_\Lambda)$. Here, $\Lambda = \{y_t\}_{t=0\dots T}$ is the trajectory ground truth, and $\mu_\Lambda, \Sigma_\Lambda$ the mean and covariance of the predicted trajectory distribution conditioned on a set of observations \mathcal{O} . Yet, predicting a trajectory’s full covariance matrix Σ_Λ demands high computational resources. The $TD \times TD$ covariance matrix has to be inverted in the loss computation. To keep the computation manageable, we never compute the distribution

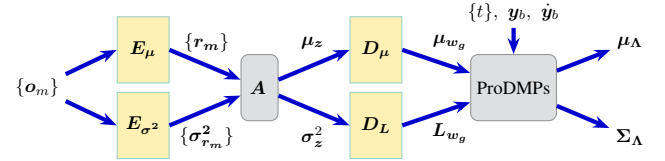


Fig. 4: Architecture and pipeline of our deep ProDMPs model. The encoders, aggregator and decoders are denoted by E , A , and D respectively. Yellow nodes denote deep neural networks, while gray nodes denote operations without learnable parameters.

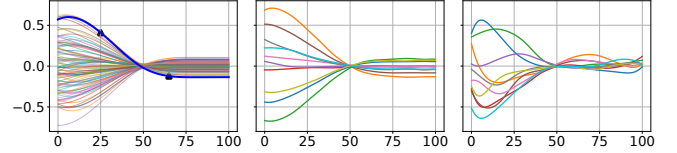


Fig. 5: Illustration of learning trajectory’s temporal correlation using two time steps. Left: Trajectories in a dataset containing temporal correlation, which can be learned through two randomly selected time steps (triangle markers). Middle: Using two time steps jointly in Eq.(19) captures the temporal correlation correctly in the inference result. Right: Maximizing the likelihood of one single time step’s value cannot learn the temporal correlation properly.

of the whole time sequence, but only compute the covariance of a pair of time steps, which limits the size of covariance matrices to $2D \times 2D$. We randomly select J such time pairs $\{(t, t')_j\}_{j=1, \dots, J}$, where $t, t' \in \{0, \dots, T\}$, and predict the joint distribution on each of these pairs. As such random selection is executed in every training batch, we can still learn the correlation between time steps while keeping the cost of matrix inversion manageable. Given the boundary conditions y_b, \dot{y}_b and a set of observations \mathcal{O} , the loss function is thus defined as the mean negative log-likelihood of J random pairs of trajectory values $y_{(t, t')_j}$ as

$$\mathcal{L}_\theta(\Lambda, y_b, \dot{y}_b, \mathcal{O}) = -\frac{1}{J} \sum_{j=1}^J \log \mathcal{N}(y_{(t, t')_j} | \mu_{(t, t')_j}, \Sigma_{(t, t')_j}), \quad (19)$$

where $\mu_{(t, t')_j}$ and $\Sigma_{(t, t')_j}$ denote the mean and covariance of the joint distribution at the j -th paired time points which are obtained from the ProDMPs decoder depicted in Figure

4. In Fig. 5, we illustrate that our loss function can capture the temporal correlation. Further, an ablation study that only computes the likelihood of single-time steps results in a degenerated estimate of the temporal correlation.

V. EXPERIMENTS

We highlight the advantages of our model and distinguish it from other methods through three experiments, which answer the following questions: (a) Does our model produce high-quality trajectory distributions and samples using non-linear conditioning on high dimensional observations? (b) Does it support online replanning and predicting a smooth trajectory distribution from the current robot state? (c) Can we condition on several partial observations and obtain a trajectory distribution that leverages the aggregated information? We compare our method with state-of-the-art CNMPs [13] and NN-based DMPs models [9–11] on three digit-writing tasks using images as inputs, one simulated robot pushing task with complex physical interaction, and a real robot picking task with shifting object positions.

A. Learning Trajectory Distributions of the MNIST Digits

We use a synthetic-MNIST dataset [10] to showcase several properties of our method and advantages over the other approaches. The dataset contains 20,000 digit images in ten groups (0-9) and as prediction targets 3 seconds trajectories with 2 DoFs each. In our settings, we choose to use 25 basis functions per DoF and predict a 52-dim multivariate Gaussian distribution over ProDMPs parameters (25 weights and 1 goal for each DoF). A 2-dim vector for the starting point of the trajectory is also predicted. We analyse our experiments based on three subtasks and show the spatial writing trajectories, i. e., the x- and y-axis are spatial DoFs.

Comparison of Generative Models. As first task, we consider the prediction of trajectories using different methods given one image input. For CNMPs and ProDMPs, we initially predict a distribution and then sample trajectories from it. As shown in Fig. 6, CNMPs only model the mean and the isotropic variance per time step and thus fail to model correlations across time steps and dimensions. The NN-DMPs instead predicted a smooth trajectory, but do not learn any statistics over the trajectories and cannot generate samples. Our model, however, not only captures the correct shape of the trajectory but can also be used as a generative model to sample temporal and DoFs consistent trajectories. To evaluate the speed of a full learning experiment, we replace the numerical integration of the NN-DMPs with our linear basis function model and keep the network architecture and MSE loss unchanged. The whole training time is reduced from 105 minutes to 10 minutes, which is approximately a speed-up by a factor of 10.

Conditioning on Partial Observations. For the second task, we show how our model leverages Bayesian Aggregation to deal with multiple partial observations. We repeatedly add synthetic noise to each original image such that we obtain three noisy images for each digit. The random noise masks occlude most of the image, leaving only a few original

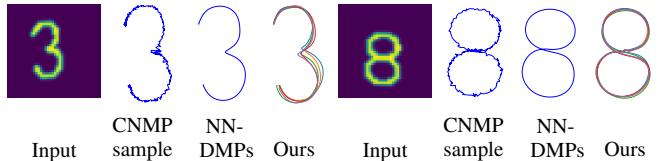


Fig. 6: The trajectories generated by different MP models. Only our model captures the temporal and DoF correlations.

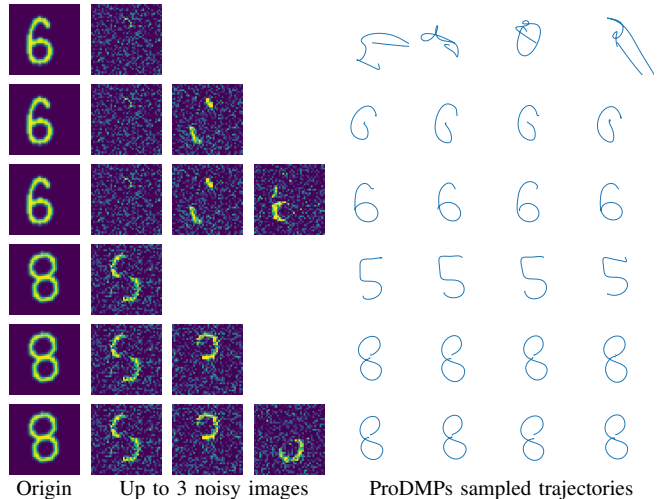


Fig. 7: Given up to three noisy images, our ProDMPs model aggregated the information and refined its prediction.

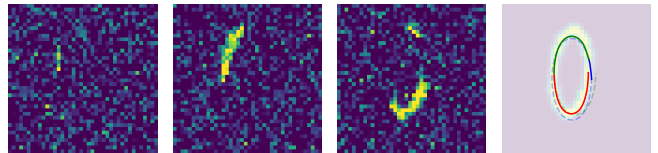


Fig. 8: Write a digit in 3 steps. Our model received the first noisy image at the beginning while receiving the second and third at 25% and 50% of the execution time respectively. The trajectory gets replanned (blue \rightarrow green \rightarrow red) and executed accordingly. The dashed lines indicate the remaining, not executed trajectories.

pixels visible. Our model successfully aggregated the information contained in the different observations and provided a trajectory distribution refinement over the predicted digit. Fig. 7 shows that the trajectories appear random without sufficient information about the digit, but become refined once more information is added.

Online Replanning. Finally, we show how our method benefits from its dynamical system in online replanning once new information is provided. To this end, we provide new observations to the method during the execution of the trajectory. The same noisy images as in the previous experiment of the target digit are provided at 0%, 25%, and 50% of the execution time. For illustration purposes, we trained the models only on images containing one type of digit. As shown in Fig. 8, each additional observation increases the accuracy of the trajectory, while the new trajectories transition smoothly at the replanning points.

B. Pushing and Replanning with Complex Contact

We conduct a simulated robot experiment to prove that our approach can deal with rich physical interactions and online conditioning on environmental variables. We use a Franka Panda robot in Mujoco [26] to push a box with its end-effector (cf. Fig. 9). The box has a square shape and is empty. The end-effector is equipped with a peg and starts in the box. Using a simple teleoperation interface, we control the end-effector’s x and y position with a mouse, which is then translated into the joint angles using inverse kinematics (IK). We collected 225 demos, each 3 seconds long, moving the box from a random initial state to a desired target position and orientation. The box is hard to control, especially the orientation, due to the non-linear interaction of its walls and corners with the peg. The learning procedure is as follows. At each iteration, we randomly choose a replanning time point and use the recorded box position, orientation, as well as the actual position and velocity of the robot end-effector in the past 0.1s as observations. We predict a desired end-effector trajectory distribution in the next 0.5s, using ProDMPs with 25 basis functions per DoF, and maximize the log-likelihood of the demonstrated trajectory. In the inference phase, our model directly interacts with the simulator, pushing a box from an unseen initial state. We executed either the mean or the sampled trajectory of the predicted trajectory distribution. We compare our method with (a) CNMPs only using the mean, (b) CNMPs with sampling, (c) ablated ProDMPs without replanning, and (d) a vanilla behavior cloning network mapping observations to actions at each time step.

We evaluate the error between the final and target states of the box, as well as the average squared acceleration (ASA, the smaller the better) as a trajectory smoothness metric. The result is shown in Table II. Our model can reproduce the box-pushing task with similar accuracy as the demos and achieves excellent levels of smoothness. The performance of the CNMPs’ mean prediction yields a similar pushing result to our model. However, the trajectory samples are, as expected, unable to solve the task. In addition, CNMPs exhibit noticeable jumps and significant accelerations at the transition points of the trajectory. The sampled trajectories are lacking temporal and DoFs correlation, leading to an extremely low level of smoothness. The ablated case of our model cannot solve the task properly, indicating that replanning is crucial to adjust the movement in such a contact-rich scenario. The comparably high smoothness is achieved by the lack of replanning in the trajectory. The state-action-based behavioral cloning using an MSE loss cannot capture the temporal correlation between the box and the robot’s movement, and thus performs poorly. It is worth mentioning that using NN-based DMPs in the current task is equivalent to training our model with the MSE loss, which will lead to the same result but a faster speed.

C. Object Picking with Dynamic Positional Shift

Finally, we learn an object-picking task in a 7-DoFs joint space. A Franka Panda robot picks an object in its workspace

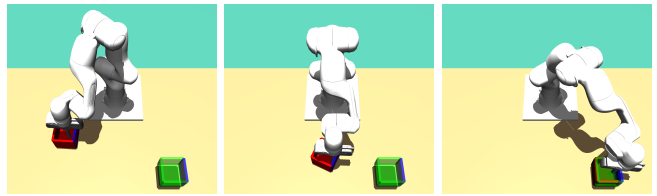


Fig. 9: Pushing an empty box (red) from a randomized initial state to a given target position and orientation (green) in Mujoco [26].

TABLE II: Evaluation of different settings using (a) Mean and std of the absolute error (x -/ y -position and orientation along z -axis) of the final box state to its target state, as well as (b) the average squared acceleration (ASA) as smoothness metric. Each model is trained 20 times using different random seeds.

	Replan	x (mm)	y (mm)	z -ori. (deg)	ASA
Demos	-	4.2 ± 2.9	4.8 ± 3.4	1.76 ± 1.28	-
ProDMP	mean	9.2 ± 8.2	7.1 ± 7.2	4.3 ± 5.7	3.3
CNMP	mean	9.5 ± 9.2	7.5 ± 9.7	4.7 ± 9.0	800.5
ProDMP	sample	19.0 ± 31.3	17.6 ± 20.1	12.1 ± 21.1	13.1
CNMP	sample	72.4 ± 13.7	80.8 ± 21.5	20.8 ± 14.4	2.7e4
ProDMP	\times	62.0 ± 53.9	55.9 ± 38.8	33.6 ± 28.4	0.3
B. C.	per step	35.8 ± 34.0	94.9 ± 14.2	21.2 ± 24.0	7.1

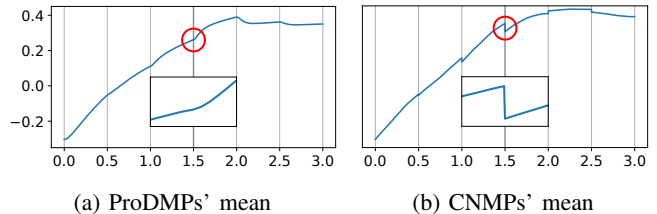


Fig. 10: Replanning trajectories comparison of robot pushing. x -axis: time [s], y -axis: end-effector y position [m]. Each trajectory is a concatenation of 6 replanning segments, 0.5 second long each. Our model is smooth at the replanning time steps (vertical lines), while the CNMPs are discontinuous when replanning.

(cf. Fig. 11a). During execution, the object shifts to a new position, and the robot must plan a new trajectory from its current position to pick up the object without interruption. We collected 100 human demos, each 4 seconds long, using the same teleoperation interface as in Section V-B. In each demo, the human moves the robot end-effector to the object and adjusts the movement when the object shifts. The demonstrated joint trajectory is computed using IK. After each second, the actual object position and the robot state are given to ProDMPs to replan a trajectory distribution starting from the current robot state. We evaluated the picking success rate of our model using the (a) mean prediction, and (b) trajectory samples in a simulated and a real setup. The box position in the real setup is captured by a camera system using ArUco ROS [27]. Our model learns picking and replanning movement directly from the data and achieves a high success rate in simulation, as shown in TABLE III. Due to the camera delay in the real setup, the performance decreases slightly. Fig. 11b shows four predicted trajectory distributions in one sequence. Our model predicts the trajectory distribution with

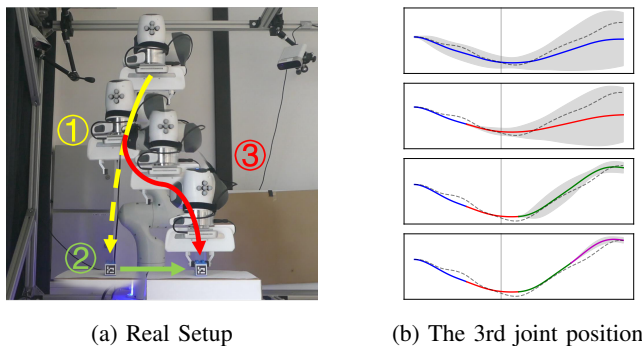


Fig. 11: (a) The robot is picking an object initialized on the left. During the movement, the object was shifted to the right, and the robot replanned a new trajectory from its current state to the new object position without interruption. (b) For each episode, every 1 second our model predicts a new distribution using its current state and the latest box position. Before the shift (vertical line), the predictions contain high variance. After the shift, the variance decreases intensely. The dashed line denotes the human’s demo.

TABLE III: Success rate and shift distance of 100 picks

100 picks of	Sim+mean	Sim+sample	Real+mean	Real+sample
Success rate	99%	82%	87%	75%
Shift distance	22.8 \pm 5.6		21.7 \pm 9.7	21.0 \pm 8.0

a high variance at the beginning and decreases the predicted variance once it observes the shift of the object.

VI. CONCLUSION

We presented ProDMPs, a unified framework fusing dynamic and probabilistic movement primitives. ProDMPs recovered a linear basis-function representation for the trajectories by solving the ODE of the dynamical system. This way, we can easily represent trajectory distributions that adhere to boundary conditions defined by the current robot position and velocity as well as generate smooth trajectories when replanning. Further, we built a neural aggregation model for non-linear iterative conditioning and found a solution to learn full trajectory covariances with fewer resources. Our deep embedded ProDMPs achieved smoothness, goal convergence, trajectory correlation modeling, non-linear trajectory conditioning, and online replanning in one model. For future work, we will extend our approach to reinforcement learning, also considering force profiles that need to be applied.

VII. ACKNOWLEDGEMENT

The authors acknowledge support by the state of Baden-Württemberg through bwHPC.

REFERENCES

- [1] S. Schaal. “Dynamic movement primitives—a framework for motor control in humans and humanoid robotics”. In: *Adaptive motion of animals and machines*. Springer, 2006, pp. 261–280.
- [2] A. Paraschos, C. Daniel, J. R. Peters, and G. Neumann. “Probabilistic movement primitives”. In: *Advances in neural information processing systems* 26 (2013).
- [3] G. J. Maeda, G. Neumann, M. Ewerton, R. Lioutikov, O. Kroemer, and J. Peters. “Probabilistic movement primitives for coordination of multiple human–robot collaborative tasks”. In: *Autonomous Robots* 41.3 (2017), pp. 593–612.

- [4] Y. Zhou, J. Gao, and T. Asfour. “Learning via-point movement primitives with inter-and extrapolation capabilities”. In: *2019 IEEE/RSJ International Conference on Intelligent Robots and Systems (IROS)*. IEEE, 2019, pp. 4301–4308.
- [5] O. Celik, D. Zhou, G. Li, P. Becker, and G. Neumann. “Specializing Versatile Skill Libraries using Local Mixture of Experts”. In: *Conference on Robot Learning*. PMLR, 2022, pp. 1423–1433.
- [6] G. Maeda, M. Ewerton, G. Neumann, R. Lioutikov, and J. Peters. “Phase estimation for fast action recognition and trajectory generation in human–robot collaboration”. In: *The International Journal of Robotics Research* 36.13-14 (2017), pp. 1579–1594.
- [7] F. Otto, O. Celik, H. Zhou, H. Ziesche, V. A. Ngo, and G. Neumann. “Deep Black-Box Reinforcement Learning with Movement Primitives”. In: *6th Annual Conference on Robot Learning*.
- [8] A. J. Ijspeert, J. Nakanishi, H. Hoffmann, P. Pastor, and S. Schaal. “Dynamical movement primitives: learning attractor models for motor behaviors”. In: *Neural computation* 25.2 (2013), pp. 328–373.
- [9] A. Gams, A. Ude, J. Morimoto, et al. “Deep encoder-decoder networks for mapping raw images to dynamic movement primitives”. In: *2018 IEEE International Conference on Robotics and Automation (ICRA)*. IEEE, 2018, pp. 5863–5868.
- [10] B. Ridge, A. Gams, J. Morimoto, A. Ude, et al. “Training of deep neural networks for the generation of dynamic movement primitives”. In: *Neural Networks* 127 (2020), pp. 121–131.
- [11] S. Bahl, M. Mukadam, A. Gupta, and D. Pathak. “Neural dynamic policies for end-to-end sensorimotor learning”. In: *Advances in Neural Information Processing Systems* 33 (2020), pp. 5058–5069.
- [12] A. Paraschos, C. Daniel, J. Peters, and G. Neumann. “Using probabilistic movement primitives in robotics”. In: *Autonomous Robots* 42.3 (2018), pp. 529–551.
- [13] M. Y. Seker, M. Imre, J. H. Piater, and E. Ugur. “Conditional Neural Movement Primitives.” In: *Robotics: Science and Systems*. Vol. 10. 2019.
- [14] F. Brandherm, J. Peters, G. Neumann, and R. Akrou. “Learning replanning policies with direct policy search”. In: *IEEE Robotics and Automation Letters* 4.2 (2019), pp. 2196–2203.
- [15] M. Saveriano, F. J. Abu-Dakka, A. Kramberger, and L. Peternel. “Dynamic movement primitives in robotics: A tutorial survey”. In: *arXiv preprint arXiv:2102.03861* (2021).
- [16] M. Volpp, F. Flürenbrock, L. Grossberger, C. Daniel, and G. Neumann. “Bayesian context aggregation for neural processes”. In: *International Conference on Learning Representations*. 2020.
- [17] S. Calinon, Z. Li, T. Alizadeh, N. G. Tsagarakis, and D. G. Caldwell. “Statistical dynamical systems for skills acquisition in humanoids”. In: *2012 12th IEEE-RAS International Conference on Humanoid Robots (Humanoids 2012)*. IEEE, 2012, pp. 323–329.
- [18] C. Yang, C. Chen, W. He, R. Cui, and Z. Li. “Robot learning system based on adaptive neural control and dynamic movement primitives”. In: *IEEE transactions on neural networks and learning systems* 30.3 (2018), pp. 777–787.
- [19] F. Meier and S. Schaal. “A probabilistic representation for dynamic movement primitives”. In: *arXiv preprint arXiv:1612.05932* (2016).
- [20] H. B. Amor, G. Neumann, S. Kamthe, O. Kroemer, and J. Peters. “Interaction primitives for human-robot cooperation tasks”. In: *2014 IEEE international conference on robotics and automation (ICRA)*. IEEE, 2014, pp. 2831–2837.
- [21] M. Garnelo et al. “Conditional neural processes”. In: *International Conference on Machine Learning*. PMLR, 2018, pp. 1704–1713.
- [22] G. Teschl. *Ordinary differential equations and dynamical systems*. Vol. 140. American Mathematical Soc., 2012.
- [23] M. Akbulut, E. Oztop, M. Y. Seker, X. Hh, A. Tekden, and E. Ugur. “Acnmp: Skill transfer and task extrapolation through learning from demonstration and reinforcement learning via representation sharing”. In: *Conference on Robot Learning*. PMLR, 2021, pp. 1896–1907.
- [24] M. Zaheer, S. Kottur, S. Ravanbakhsh, B. Poczos, R. R. Salakhutdinov, and A. J. Smola. “Deep sets”. In: *Advances in neural information processing systems* 30 (2017).
- [25] M. Garnelo et al. “Neural processes”. In: *arXiv preprint arXiv:1807.01622* (2018).
- [26] E. Todorov, T. Erez, and Y. Tassa. “Mujoco: A physics engine for model-based control”. In: *2012 IEEE/RSJ international conference on intelligent robots and systems*. IEEE, 2012, pp. 5026–5033.
- [27] R. Salinas and B. Magyar. *ArUco ROS library*. 2015.

APPENDIX I
ILLUSTRATION OF TRAJECTORY COVARIANCE
PREDICTION

We present two intuitive examples to illustrate (a) how do different approaches model trajectory covariance, (b) how does our model learn covariance in an affordable way.

A. Modeling Trajectory Covariance

We follow the definition of trajectory covariance used in the ProMPs [2], i.e., trajectory values of different DoFs at different time steps are coupled and modeled in one multi-variate distribution, which differs from the mixture models, such as GMM/GMR-DMP [17, 18], where multiple Gaussian distribution components are used to cover the demonstrated trajectories' domain. We illustrate an element-wise trajectory distribution example in Fig. 12. The diagonal elements of the covariance matrix (colored in red) indicate the isotropic variance of the trajectory, while the remaining elements represent the covariance between time-steps and between different DoFs. The original ProMPs and our ProDMPs use a linear basis function model and can model the entire covariance matrix given $p(\mathbf{w}_g) \sim \mathcal{N}(\mathbf{w}_g | \boldsymbol{\mu}_{w_g}, \boldsymbol{\Sigma}_{w_g})$. Recent approaches such as CNMPs [13] and NDPs [11] (RL part), however, can only model the isotropic trajectory variance (elements in red shadow in Fig. 12). The correlation between different DoFs, and between time steps is missing. Therefore,

their predicted trajectory distribution cannot sample time and DoFs-consistent new trajectories without further smoothness, which explains the reason for the noisy samples in Fig. 6.

B. Make Full Covariance Learning Affordable

As briefly introduced in Section IV, learning all time steps' covariance whose size is $TD \times TD$, requires a high resource demand. Such a high resource demand is often not feasible for a deep NN model, where multiple trajectories are often learned in a batched manner, and the computational graph shall be stored for back-propagation usage. Therefore, to make the learning feasible, we randomly select a group of paired time steps, each pair having a $2D \times 2D$ covariance, and optimize the trajectory values' joint distribution. As illustrated in Fig. 13, learning a distribution of paired time steps is equivalent to learning a sub-vector and a sub-matrix of the original ones. As such time pairs are randomly selected in different mini-batches, the original covariance matrix will be learned eventually.

APPENDIX II
EXPERIMENT HYPER-PARAMETERS SETTINGS

The hyper-parameters of our experiments and neural network architectures are listed in TABLE IV - VIII respectively.

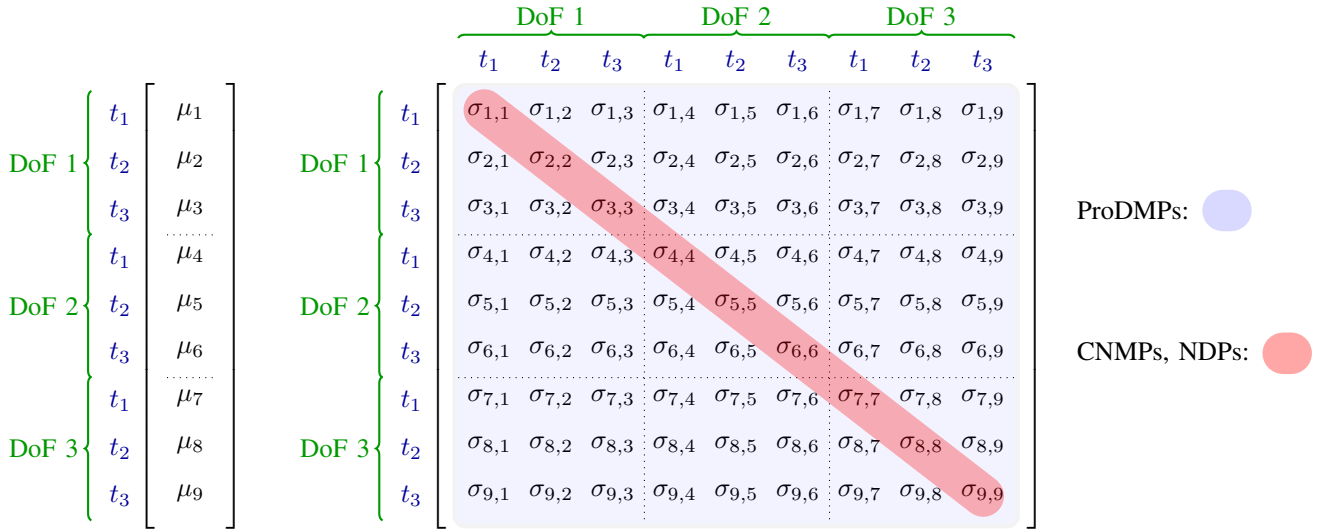


Fig. 12: Element-wise representation of a multi-variant Gaussian distributed trajectory. This example trajectory has coupled 3 time steps and 3 DoFs. Left: the trajectory mean vector. Right: the trajectory covariance matrix. We add time steps labels (t_1, t_2, t_3) and DoFs labels (DoF1, DoF2, DoF3) to indicate each element's meaning, e.g. μ_5 is the trajectory mean value of the 2nd DoF at the 2nd time step, and $\sigma_{1,9}$ represents the covariance between the trajectory value of the 1st DoF at the 1st time step and the trajectory value of the 3rd DoF at the 3rd time step. Our method learns the entire trajectory covariance matrix (elements in light blue), while the other method [11, 13] learns only the isotropic variance (elements red).

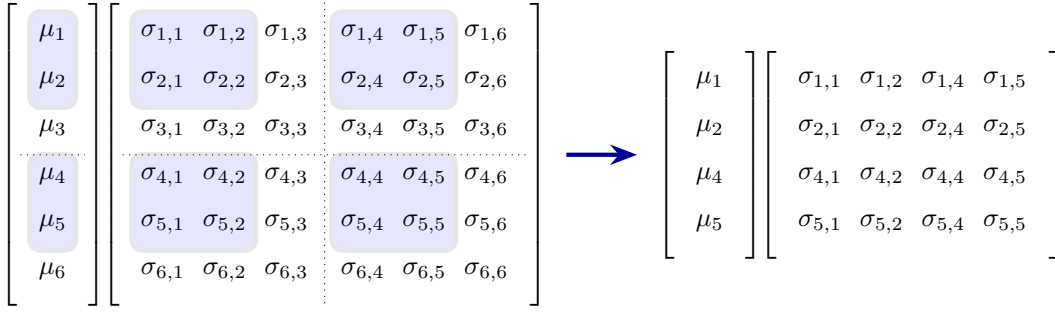


Fig. 13: An illustration of learning full covariance through paired time steps. **Left:** This example trajectory has coupled 3 time steps and 2 DoFs. Here we omit the time-step and DoF labels for simplicity. **Right:** We randomly select 2 time steps, e.g. t_1, t_2 , form up a pair, and learn their joint distribution, which is equivalent to learn a sub-vector and a sub-matrix of the original ones.

TABLE IV: Experiment settings of writing digit given one original image.

Settings	CNMPs	NN-based DMPs	ProDMPs
Input obs.	One original digit image, size: 40×40		
Predict	Traj. mean and std	DMPs weights + goal	Mean + cov of ProDMPs weights
Form up trajectory	-	Numerical integration	Use linear basis function in Eq. (11)
Loss func.	Traj. NLL	Traj. MSE	Traj. LL-loss in Eq. (19)
Traj. sampling	From traj. distribution	\times	First sample weights then use linear basis function Eq. (11)
No. of Basis	-	25 per DoF	25 + 1 (weights + goal) per DoF
No. of DoFs	2 in task space		
Type of Basis	-	RBF	RBF
Hyper-params.	Optimizer: [Adam, learning rate: $2e-4$, weights decay: $5e-5$] Dim of latent obs.: 128. DMPs: [α_x : 2, α : 25, τ : 3]		
Obs. encoder Unc. encoder in Fig. 4	{ CNN: [kernel: 5, stride: 1, channel in: 1, channel out: 10] Max pooling: [kernel: 2, stride: 2, channel in: 10, channel out: 10] CNN: [kernel: 5, stride: 1, channel in: 10, channel: out: 20, dropout: 0.5] Max pooling: [kernel: 2, stride: 2, channel in: 20, channel out: 20] MLP: [input neurons: 980, hidden: [128, 128, 128], output: 128] }		
Mean. dec. Unc. dec. in Fig. 4	ProDMPs Mean: MLP[input: 128, hidden: [128, 128, 128], output: 54] ProDMPs Cov: MLP[input: 128, hidden: [256, 256, 256, 256], output: 1485] CNMPs Mean: MLP[input: 128 + 1, hidden: [128, 128, 128], output: 2] NN-DMPs Mean: MLP[input: 128, hidden: [128, 128, 128], output: 54]		

TABLE V: Experiment setting of writing digit given at most 3 noisy images.

Settings	ProDMPs
Input observation	One, two, or three noisy digit images generated from the original image
Predict	Mean and covariance of ProDMPs weights
Form up trajectory	Use linear basis function in Eq. (11)
Loss func. Traj.	LL-loss in Eq. (19)
Traj. sampling	First sample weights, then use linear basis function Eq. (11)
No. of Basis and DoFs	25 + 1 per DoF, 2 DoFs in task space, type: RBF
Hyper-params.	Optimizer: [Adam, learning rate: $2e-4$, weights decay: $5e-5$] Gradient clipping norm: 20. Dim of latent obs.: 128. DMPs: [α_x : 2, α : 25, τ : 3]
Encoders and Decoders	Same as Table IV

TABLE VI: Experiment setting of writing digit in 3 steps.

Settings	ProDMPs using sub-datasets containing 1 type of digit
Input observation	One, two, or three noisy digit images generated from the original image
Predict	Mean and covariance of ProDMPs weights
Form up trajectory	Use linear basis function in Eq. (11) Use the execution of the previous prediction at 0%, 25% and 50% respectively as boundary condition
Loss func. Traj.	LL-loss in Eq. (19)
No. of Basis	25 + 1 per DoF
No. of DoFs	2 in task space
Type of Basis	RBF
Hyper-params.	Optimizer: [Adam, learning rate: 2e-4, weights decay: 5e-5] Gradient clipping norm: 20. Dim of latent obs.: 128. DMPs: [α_x : 2, α : 25, τ : 3]
Encoders and Decoders	Same as Table IV

TABLE VII: Experiment settings of robot pushing task.

Settings	CNMPs	ProDMPs
Input obs.	The box and robot's actual state in the past 0.1 second	
Predict	Traj. mean and std of next 0.5s	Mean + cov of ProDMPs weights in the next 0.5s
Form up trajectory	-	Use linear basis function in Eq. (11)
Loss func.	Traj. NLL	Traj. LL-loss in Eq. (19)
Traj. sampling	From traj. distribution	First sample weights then use linear basis function Eq. (11)
No. of Basis	-	25 + 1 per DoF
No. of DoFs	2 in task space	
Type of Basis	-	RBF
Hyper-params.	Optimizer: [Adam, learning rate: 2e-4, weights decay: 5e-5] Dim of latent obs.: 128. DMPs: [α_x : 0.5, α : 25, τ : 0.5]	
Settings	ProDMPs no replanning	Behaviour Cloning
Input obs.	The initial box and robot state	The latest actual box and robot state
Predict	Mean + cov of ProDMPs weights of the entire traj.	Robot's desired one-step trajectory
Form up trajectory	Use linear basis function in Eq. (11)	-
Loss func.	Traj. LL-loss in Eq. (19)	MSE loss
No. of Basis	25 + 1 per DoF	-
No. of DoFs	2 in task space	
Type of Basis	RBF	-
Hyper-params.	Optimizer: [Adam, learning rate: 2e-4, weights decay: 5e-5] DMPs: [α_x : 3, α : 25, τ : 3]	
Encoders, decoders, and other NNs	ProDMPs Obs./Unc. enc.: MLP[input neuron: 8, hidden:[128, 128, 128], output: 128]	
	CNMPs Obs. enc.: MLP[input neuron: 8, hidden:[128, 128, 128], output: 128]	
	ProDMPs Mean. dec.: MLP[input neuron: 128, hidden:[128, 128, 128], output: 52]	
	ProDMPs Cov. dec.: MLP[input neuron: 128, hidden:[128, 128, 128], output: 1326]	
	CNMPs Mean/Std dec.: MLP[input neuron: 128+1, hidden:[128, 128, 128], output: 2]	
	Behaviour Cloning Net: MLP[input neuron: 6*, hidden:[128, 128, 128], output: 2]	
	*We found that not offering the robot actual velocity (2-dim) increases the performance.	

TABLE VIII: Experiment settings of robot picking task.

Settings	ProDMPs
Input observation	The object and robot state at the 0, 1, 2, 3 seconds
Predict	Mean and covariance of ProDMPs weights
Post-process	Use linear basis function in Eq. (11)
Loss func. Traj.	LL-loss in Eq. (19)
Traj. sampling	First sample weights then use linear basis function Eq. (11)
No. of Basis	9 + 1 per DoF
No. of DoFs	7 in joint space
Type of Basis	RBF
Hyper-params.	Optimizer: [Adam, learning rate: 2e-4, weights decay: 5e-5] Dim of latent obs.: 128. DMPs: [α_x : 3, α : 25, τ : 4]
Encoders	Obs./Unc. encoder: MLP[input neurons: 4, hidden: [64, 64, 64], output: 64]
Decoders	ProDMPs Mean: MLP[input: 64, hidden: [64, 64, 64], output: 70] ProDMPs Cov: MLP[input: 64, hidden: [64, 64, 64], output: 2415]